Compressive deformation behavior of dendritic Mg–Ca(–Zn) alloys at high temperature

Justine Papillon, Paul Salero, Florian Mercier, Damien Fabrègue, Éric Maire

Compressive deformation behavior of dendritic Mg–Ca(–Zn) alloys at high temperature

Justine Papillon[a], Paul Salero[a], Florian Mercier[a], Damien Fabrègue[a], Éric Maire[a]

[a] *Univ. Lyon, INSA Lyon, MATEIS, UMR CNRS 5510, F-69621 Villeurbanne, France*

Abstract

Mg-Ca(-Zn) alloys were subjected to hot compression at temperatures ranging from 350 °C to 450 °C and strain rates of 10^{-3} to 10 s^{-1}. In the corresponding flow curves, the peak stress appeared at very low strain rates (less than 0.05) followed by steady state at a constant stress, indicating the occurrence of dynamic flow softening, which is a typical signature of dynamic recrystallization (DRX). The DRX was greatly affected by the deformation conditions and Ca/Zn contents, and optical and scanning electron microscopy analysis revealed that the DRX induced rearrangement of the complex dendritic microstructure during compression. Optimal parameters for the deformation were identified. These indicate deformation conditions where the processing is safe and easy. This in turn is likely to enable widening of the range of applications of Mg-Ca(-Zn) alloys.

Keywords: magnesium alloys, multiphase, hot compression, dynamic recrystallization
MSEA-D-19-00936R1

Graphical abstract

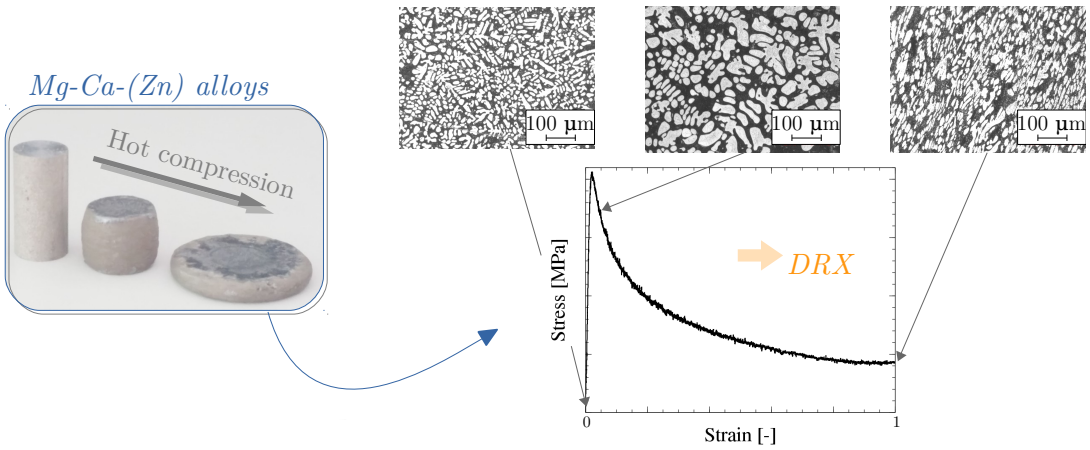

Corresponding author:
Justine Papillon
Tel: +33 4 72 43 63 81
E-mail address : justine.papillon@insa-lyon.fr
Laboratoire MATEIS
25, avenue Jean Capelle
Bâtiment Saint Exupéry
69 621 Villeurbanne Cedex
FRANCE

1. Introduction

Mg shows great potential for application in the automotive and aerospace industries because of its low density, high specific strength, high corrosion resistance, and good damping capacity, all of which are beneficial for reducing the weight of structures [1]. In addition, the excellent biocompatibility and biodegradability of Mg alloys make them excellent candidates for numerous biomedical applications. Moreover, a wide range of alloying elements such as Al, Mn, Ca, and Zn can be added to Mg to potentially improve its mechanical properties and corrosion resistance [2] [3] [4] [5]. However, Al alloys and polymer materials have long been preferred over Mg alloys as Mg alloys exhibit poor ductility at room temperature owing to their hexagonal close-packed (hcp) structure, which results in a small number of slip systems and leads to deformation incompatibilities and fracture during cold shaping [6] [7]. To improve the poor workability of Mg, it is thus of considerable interest to investigate the deformation behavior of Mg alloys at high temperatures, which facilitate Mg deformation [8].

In many recent studies, attempts have been made to understand the deformation mechanisms governing the hot compression of Mg alloy grades such as AZ31 or AZ61 [9] [10] [11] [12]. The properties of these superplastic alloys have been improved by grain refinement, which has been attributed to dynamic recrystallization (DRX) [13]. This process involves a progressive increase in the grain boundary misorientation and conversion of low-angle boundaries into high-angle boundaries [14] [15] [16].

Although the hot deformation of Mg-based alloys has been investigated for low concentrations of alloying elements and for alloys that are mostly monophasic [17] [18], very few studies have described cases in which the quantity of the alloying element addition was so large that two phases were clearly observed in the microstructure. According to the Mg/Ca equilibrium diagram, two phases can be observed when the Ca content exceeds 5 wt.%. In this case, the alloy exhibits two deformation phases. The alloy behavior at high temperatures is not very well documented in the literature. Although a few attempts have been made to study the co-deformation of multiphase alloys at high temperatures [19] [20], none of these describe the Mg–Ca system.

These alloys could be used for bone substitute and it has been shown that the microstructure influences the dissolution kinetic in body liquid [21]. It is then important to understand how the microstructure builds up during processing. The understanding of the high temperature mechanical behaviour of these alloys is also of particular interest because for biomedical application, shaping at high temperature is a key process to obtain parts adapted to the patient.

The present study focuses on the deformation behavior of Ca-rich Mg–Ca(–Zn) alloys under hot compression. The deformation behavior was investigated up to very high strains at different strain rates for varying Ca and Zn contents. Our findings highlight the interactions between the different phases, which behaved differently during deformation.

	9Ca	18,4Ca	24Ca	30Ca
∅ Zn	*	*	*	*
1Zn	*			
5Zn	*		*	

Table 1: Chemical composition (wt. %) of the Ca-Zn-rich Mg alloys studied in this paper.

2. Experimental protocol

2.1. Materials

The Ca–Zn-rich Mg alloys used in this study were received as die-cast ingots from the Korea Institute of Industrial Technology (KITECH, South Korea). The Ca contents of the Mg-based alloys were 9 wt.%, 18.4 wt.%, 24 wt.%, and 30 wt.%. In addition, the Mg–9Ca (wt.%) alloy was also tested with the addition of 1 wt.% and 5 wt.% Zn, and the Mg–24Ca (wt.%) alloy was tested with the addition of 5 wt.% Zn. The samples were investigated in as-cast condition. The chemical compositions of all the investigated alloys are summarized in Table 1.

2.2. Compression tests

Cylindrical compression samples with dimensions of ∅ 6.9 mm × H 14 mm were machined directly from the as-cast ingots using wire electrical discharge machining. Uniaxial compression tests were performed on a Gleeble 3500 thermomechanical simulator at three different temperatures (350 °C, 400 °C, and 450 °C) and five different strain rates (10^{-3}, 10^{-2}, 10^{-1}, 1, and 10 s^{-1}). The heating rate was set to 5 °C/s in all cases, and the heating stage was followed by a loading stage, during which compression was applied. The compression time depended on the strain rate and ranged between 0.2 s and 33 min.

To evaluate the microstructural evolution, some tests were interrupted at selected values of strain (as shown in Figure 1), and the samples were cut and polished for optical microscopy or scanning electron microscopy (SEM) observation. A type-K thermocouple was welded onto the surface of the sample for temperature measurements.

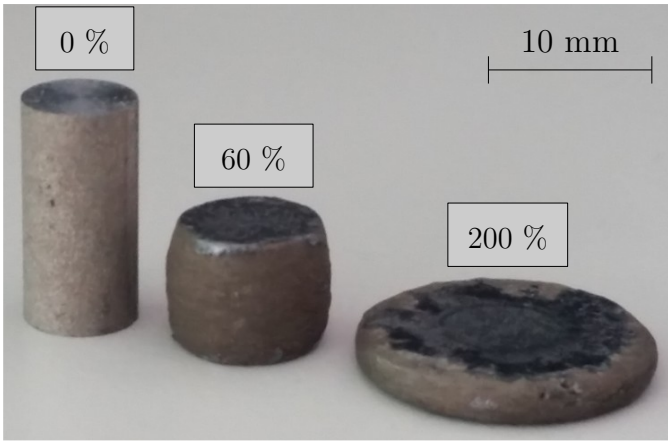

Figure 1: Specimens compressed at 400 °C/10^{-3} s^{-1} to different strain values.

2.3. Microstructural observations

The optical microscopy and SEM specimens were cut from the central area of the deformed sample in sections parallel or perpendicular to the compression axis. After polishing, the samples were etched with 4 % Nital. X-ray diffraction (XRD) was used to determine the phases present, as described by Salero [22]. The microstructural evolution was also analyzed in 3D using a dedicated X-ray tomograph (RX Solution Easy-Tom Nano [23]) and ImageJ software [24].

2.4. Vickers hardness

Hardness tests were performed with 1-kg loads to determine the macroscopic hardness of the alloy in the initial and deformed states. An average value was calculated from at least 10 measurements for each test.

3. Results

3.1. Initial microstructure

3.1.1. Effect of Ca addition

Figure 2 presents the equilibrium diagram of the Mg–Ca alloy. The following statements can be made:

- For Ca contents greater than or equal to 0 wt.% and less than 18.4 wt.%, the equilibrium microstructure should be composed of primary Mg dendrites and the lamellar eutectic aggregate Mg+Mg_2Ca. This microstructure is clearly observed in Figure 3a for the alloy containing 9 wt.% Ca, where Mg dendrites are visible (darker parts of the image).

- For a Ca concentration of 18.4 wt.%, which corresponds to the eutectic composition, the alloy should be composed of a single constituent, namely the lamellar eutectic aggregate Mg+Mg_2Ca. Although this microstructure is mainly observed in the SEM micrograph in Figure 3b, the presence of a small amount of Mg_2Ca dendrites indicates that the composition obtained was not precisely that intended when casting the alloy.

- For Ca concentrations in the range of 18.4 wt.% to 46 wt.%, the microstructure should be composed of primary Mg_2Ca dendrites and the lamellar eutectic aggregate Mg+Mg_2Ca. Our observations were consistent with these predictions (see Figure 3c and Figure 3d).

The dendrite size was several tens of micrometers, and the eutectic lamellae had a thickness of approximately 1 µm and a length of a few micrometers. The binarization of the 3D images obtained by tomography (Figure 3h) followed by connectivity measurements indicated that all the dendrites were connected.

Energy-dispersive X-ray spectroscopy (EDX) analysis combined with SEM (Figure 4) [22] was used to determine the distribution of the alloying elements. The Mg–9Ca dendrites did not contain Ca, whereas the Mg–24Ca dendrites contained both Mg and Ca.

3.1.2. Effect of Zn addition

The addition of Zn led to a more complex microstructure. Here, the eutectic aggregate was composed of Mg+Mg_2Ca+$Mg_6Ca_2Zn_3$ (Figure 3e, f and g), and the dendrites were less defined. EDX analyses showed that there was no presence of Zn in the dendrites [22]. In addition, some cracks appeared in areas that were rich in Zn.

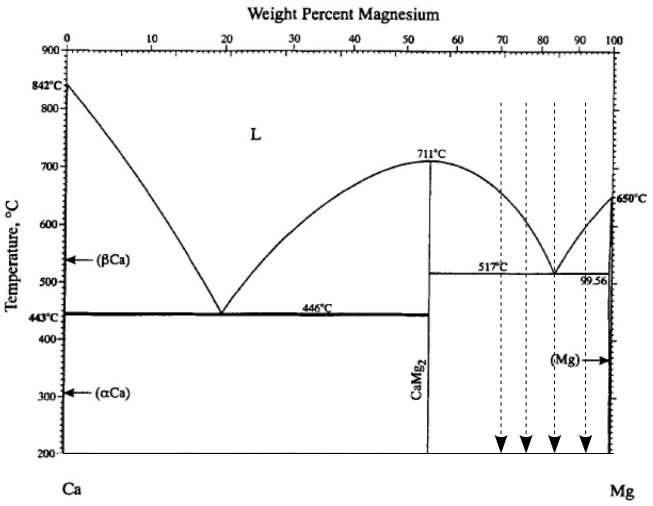

Figure 2: Mg-Ca phase diagram.

3.2. High-temperature deformation behavior

3.2.1. Effect of deformation conditions

Figure 5a presents three typical curves recorded at 350 °C, 400 °C, and 450 °C for the Mg–24Ca alloy at a strain rate of 10^{-3} s^{-1}, revealing higher levels of softening with increasing temperature, as expected. Figure 5b presents three typical curves recorded at 400 °C for the Mg–24Ca alloy at strain rates of 10^{-3}, 10^{-1}, and 10 s^{-1}. The greater softening at higher strain rates is consistent with our expectations. These results confirm the typical viscoplastic behavior of these alloys.

Compared with other curves in the literature for the same temperature range, a sharper peak was observed in this work for lower strains. However, to the best of our knowledge, no results have been published for two-phase materials.

According to the binary and the ternary diagrams of the alloys tested, at 450 °C the testing temperature does not exceed the eutectic temperature. An increase of the temperature due to the strain could be possible for high strain rate. However, we did not notice a peculiar decrease of the stress for high strain rate. Thus we strongly believe that no liquid phase is present even for the highest testing temperature.

3.2.2. Effect of initial composition

Figure 6 presents compression curves for Mg alloys with four Ca contents. The addition of Ca to the Mg alloys substantially affected the hot deformability of the alloy. With increasing Ca content, the peak strain (ε_p), peak stress (σ_p) and steady-state stress (σ_s) considerably increased, regardless of the deformation conditions. This phenomenon can be explained by the change of microstructure induced by the addition of Ca. With increasing Ca content, the replacement of the pure Mg with Mg_2Ca induced structural hardening. The alloy became stronger but also less ductile, as illustrated by the macroscopic

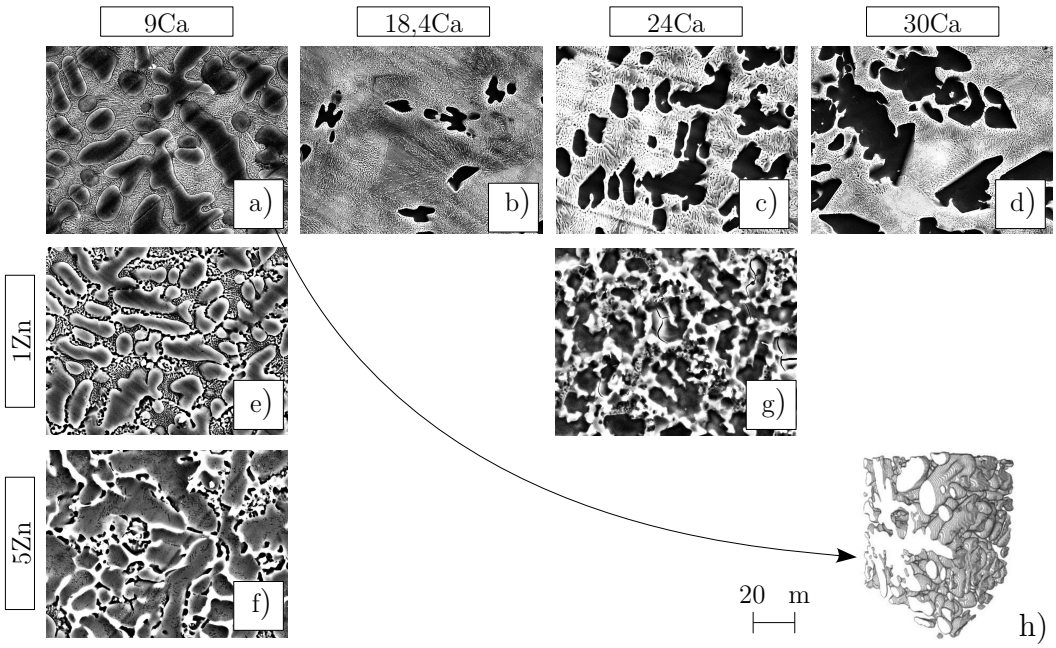

Figure 3: SEM initial micrography, in the longitudinal direction of compression, of a) Mg-9Ca; b) Mg-18.4Ca; c) Mg-24Ca; d) Mg-30Ca; e) Mg-9Ca-1Zn; f) Mg-9Ca-5Zn; g) Mg-24Ca-5Zn, and h) Tomography of Mg-9Ca.

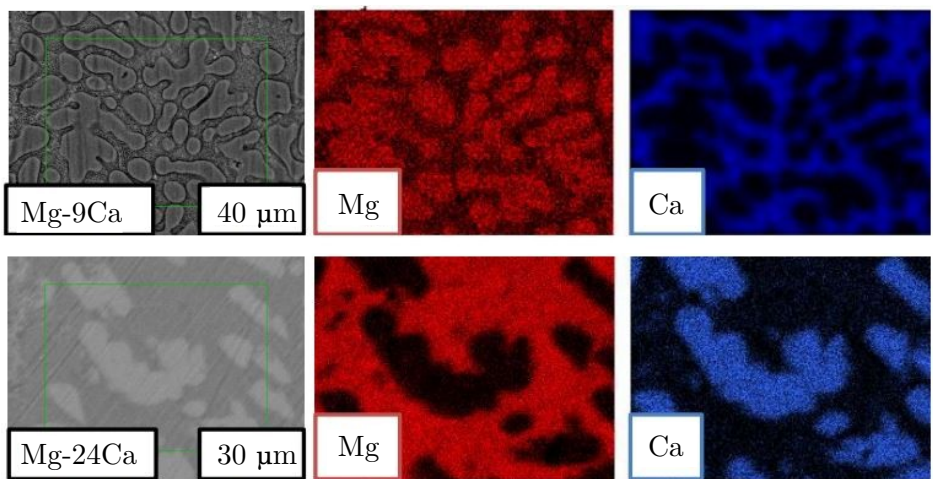

Figure 4: EDX analysis, in the longitudinal direction of compression, of Mg-9Ca and Mg-24Ca [22].

shape of the samples after deformation (Figure 6b). With increasing Ca content, the alloy thus became more brittle.

Figure 7a shows that the addition of Zn to the Mg–Ca alloy greatly affected its mechanical properties. The addition of Zn led to the appearance of $Mg_6Ca_2Zn_3$ in the microstructure, which is beneficial for structural hardening at small concentrations (1 at.%) but leads to deterioration of the mechanical properties at higher concentrations (5 at.%). Figure 7b shows the loss of ductility of the alloy when the Zn content was too high.

Concerning the peak stress, the addition of Zn appeared to promote DRX at lower levels of strain; this effect could result from the hardening effect of the $Mg_6Ca_2Zn_3$ phase, which promotes a higher dislocation density during deformation. The stress plateau appeared higher for the samples containing Zn. At low Zn content, Zn appeared in a solid solution. We can therefore consider that recrystallization will lead to the formation of smaller grains because of the slow diffusion of Zn in Mg, which would lead to a high stress plateau, as observed. For higher Zn content, the alloy contained three phases, which would lead to complex interactions that are difficult to analyze.

3.2.3. Vickers hardness

The Vickers hardness under a 1-kg load was approximately 81.7 HV for the Mg–9Ca alloy and 124.7 HV for the Mg–24Ca alloy. The hardness measured before deformation remained almost constant during the compression.

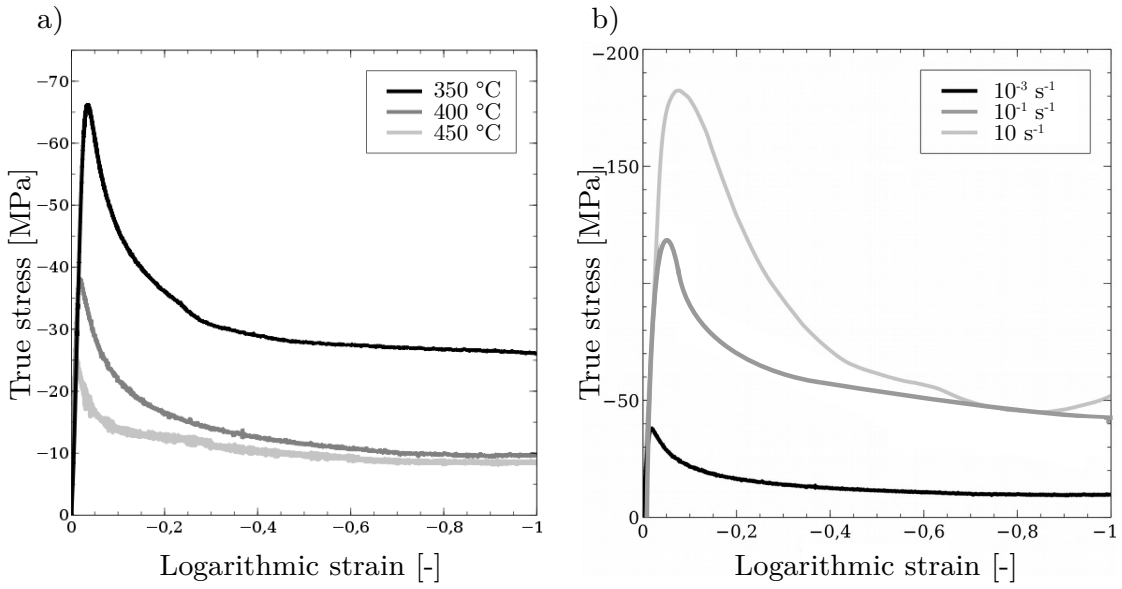

Figure 5: a) Influence of temperature at 10^{-3} s^{-1} for a Mg-24Ca alloy; b) Influence of strain rate at 400 °C for a Mg-24Ca alloy.

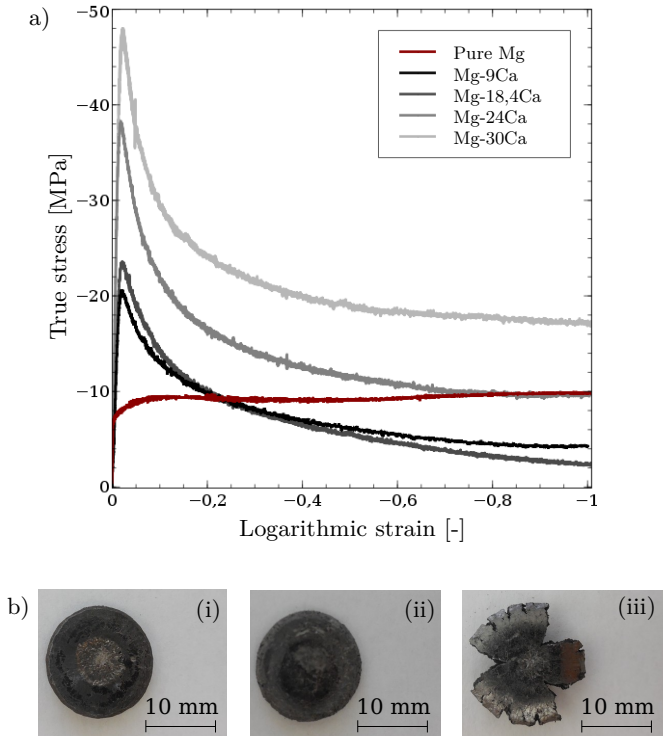

Figure 6: a) Influence of Ca at 400 °C/10^{-3} s^{-1}; b) Specimens after compression at 400 °C/10^{-1} s^{-1} at ε=2: (i) Mg-9Ca, (ii) Mg-24Ca, (iii) Mg-30Ca.

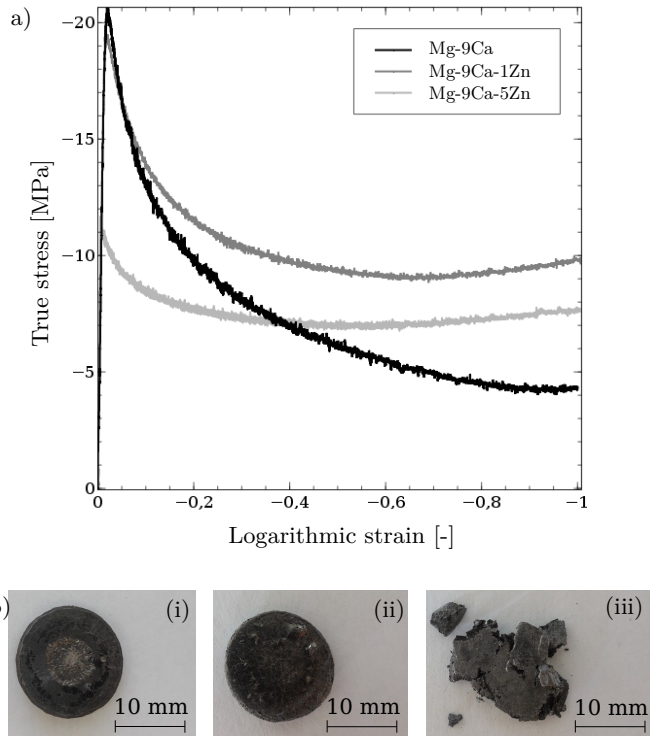

Figure 7: a) Influence of Zn at 400 °C/10^{-3} s^{-1}; b) Specimens after compression at 400 °C/10^{-1} s^{-1} at ε=2: (i) Mg-9Ca, (ii) Mg-9Ca-1Zn and (iii) Mg-9Ca-5Zn.

3.3. Dynamic recrystallization

Figure 8 presents a typical example of a flow curve obtained during the hot deformation tests. All the curves recorded during these compression tests exhibited stress–strain behavior typical of a material undergoing DRX: the flow stress rapidly increased to a peak and then rapidly decreased to a steady state because of a work-softening effect induced by recrystallization. The decrease of the stress could also be due to dynamic recovery, however, the shape of the curve and the saturation stress indicate that recrystallization have certainly taken place. DRX behavior in magnesium alloys has been previously reported in many

studies, [1] [6] [7] [8] [9] [13]. In our case, the peak occurred at very low strain levels (ε_p less than 0.05), most likely due to the dual-phase microstructure inducing a strain incompatibility between the dendrites and eutectic aggregate. A substantial amount of energy must therefore be stored at the interface during deformation, inducing early recrystallization. As the recrystallization of the Mg phase is thought to be continuous [15], its concentration in dislocations should lead to a more rapid reorganization and, thus, earlier DRX.

The important parameters used in the remainder of this study are defined in Figure 8: the peak strain (ε_p), peak stress (σ_p), and steady-state stress (σ_s).

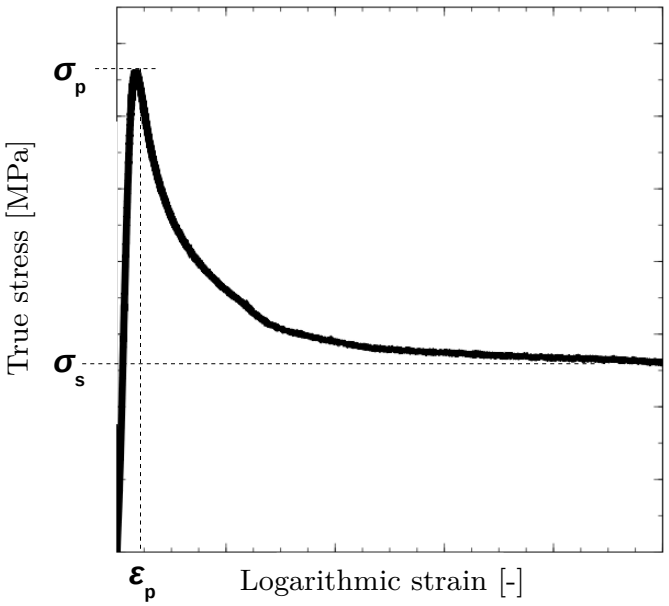

Figure 8: Typical flow curves obtained by hot compression of alloy studied.

The results were processed using an approach classically used for monophasic alloys, i.e., a Zener–Hollomon plot, according to [10]:

$$Z = \dot{\varepsilon}.e^{\frac{Q}{RT}} \quad (1)$$

where Z is the Zener-Hollomon parameter, R the gas constant, T the absolute temperature and Q, the activation energy which can be calculated with the following equation:

$$Q = n.R.\left[\frac{\delta(ln\sigma_p)}{\delta(1/T)}\right]_{\dot{\varepsilon}=constant} \quad (2)$$

and where n is the stress exponent equivalent to:

$$n = \left[\frac{\delta(ln\dot{\varepsilon})}{\delta(ln\sigma_p)}\right]_{T=constant} \quad (3)$$

The stain rate sensitivity exponent m is then equal to:

$$m = \left[\frac{1}{n}\right] \quad (4)$$

$\mathrm{Ln}(\sigma_p)$ as a function of $1/T$ was plotted, as shown in Figure 9 for a strain rate of 10^{-3} s^{-1}; the curves for other strain rates were similar but are not presented in this article. As already observed for monophasic Mg alloys, the curves $\ln(\sigma_p)$ - $1/T$ were globally linear. The slopes of these curves are summarized in the second column of the Table 2. The slope changed slightly with Ca content, and a maximum slope was obtained for the eutectic composition Mg–18.4Ca.

Alloy	$\delta(\ln\sigma_p)/\delta(\frac{1}{T})$	m	Q [kJ/mol]
Pure Mg	2,96	0,152	120,1
Mg-9Ca	1,18	0,195	102,4
Mg-18,4Ca	6,63	0,215	204,7
Mg-24Ca	4,36	0,181	146,7
Mg-30Ca	4,79	0,177	152,7

Table 2: $\delta(\ln\sigma_p)/\delta(\frac{1}{T})$ at 10^{-3} s^{-1}, strain-rate sensitivity exponent m at 400 °C and average activation energy average at 400 °C.

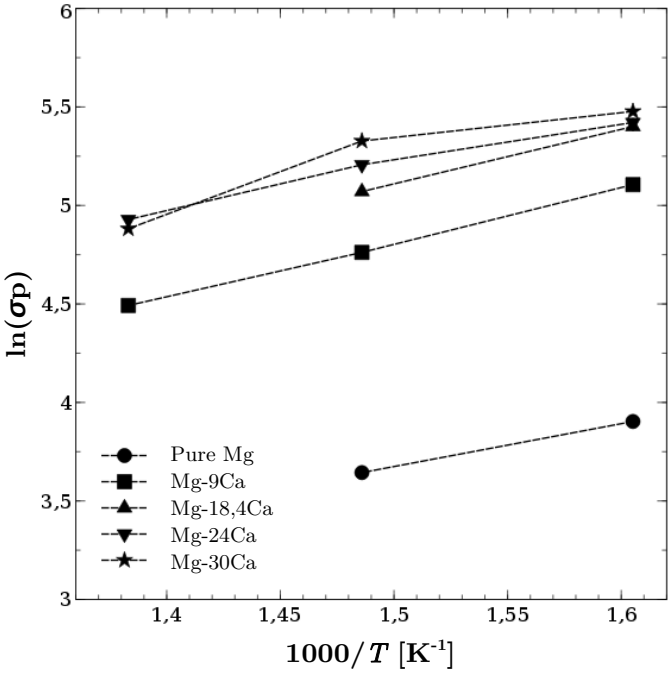

Figure 9: $1000/T$ – $\ln(\sigma_p)$ at a constant strain rate of 10^{-3} s^{-1}.

We also plotted the curves $\ln(\dot{\varepsilon})$ - $\ln(\sigma_p)$ to highlight the effect of the strain rate. Data have been determined for all temperature tested but only the results for 400 °C are presented in Figure 10. The linearity of these curves was not as obvious as for monophasic alloys, indicating that the dual-phase nature of the material plays a perturbation role here. The effect appears to be a lower peak stress at high strain rates than that predicted by a linear relation. This effect may result from the connectivity of the two phases present in the material or can be explained by the stress concentration and interfaces inducing DRX for lower macroscopic stresses. Moreover, for the Mg18.4–Ca alloy (100% eutectic alloy), recrystallization in the lamellar eutectic must be more complicated because of the smaller number of grains. This phenomenon could explain the higher activation energy Q and the higher strain-rate sensitivity exponent m for this grade summarized in Table 2. m, equivalent to the in-

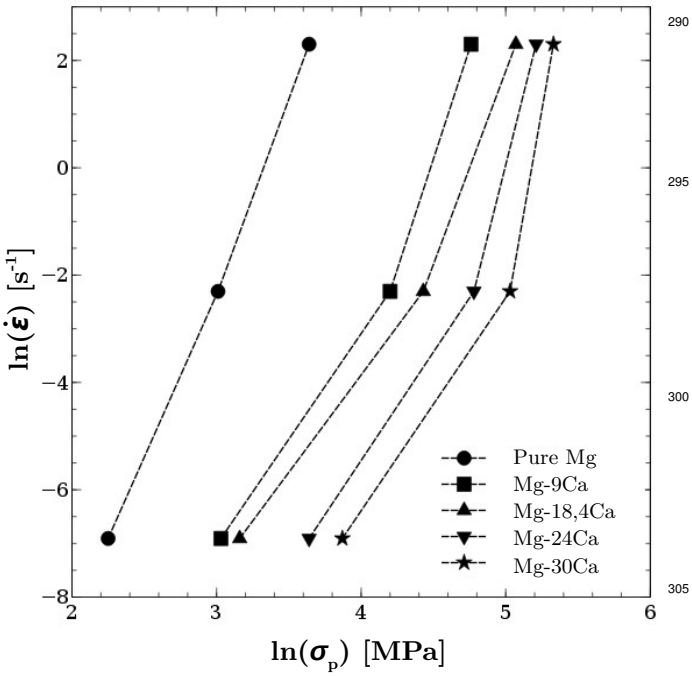

Figure 10: $\ln(\sigma_p)$ - $\ln(\varepsilon)$ at a constant temperature of 400 °C.

verse of the slopes of the curves $\ln(\dot{\varepsilon})$ - $\ln(\sigma_p)$, is equal, for the other grades, to approximately 0,152-0.195, which is similar to that measured by *Tong et al.* for a Mg–Zn–Ca alloy [3]. The Zener–Hollomon parameter is therefore a satisfactory means to identify the thermoactivation of this phenomenon.

The values of Q, averaged at 400 °C and summarized in the fourth column of Table 2, were obtained from Equation 2.

3.4. Microstructural development during hot deformation

Figure 11 shows the evolution of the Mg dendrite size in the Mg–9Ca alloy during compression at 400 °C and 10^{-3} s^{-1} with optical micrographs in the longitudinal direction of compression.We did not find any major difference in the microstructure of the alloys between the longitudinal and transverse directions at the initial state. The dimensions of the dendrites are the same in both directions of observation. During compression, differences then appear between the two directions of observation as the dendrites appear deformed only in the longitudinal direction. The DRX phenomenon that appears at the beginning of the compression led to a significant increase in the size of the dendrites (strain of 0.05). The effect appears to be a lower peak stress at high strain rates than that predicted by a linear relation. Upon further increasing the strain, the size of the dendrites tended to remain stable and even decreased at very high strain rates.

3.5. Formability map

Figure 12 presents a formability map of the alloys with temperature and strain rate. The map indicates (using colored dots) if the compression of the alloy proceeded correctly without breakage. The results described in this paper help to provide a better idea of the optimum parameters required to achieve hot deformation without brittle fracture issues. For low strain rates, the DRX has time to occur and, thus, the formability is high, regardless of the alloy. At a high strain rate, strain incompatibility at the interface between dendrites and the eutectic aggregate leads to premature fracturing of the interface before any recrystallization can occur, resulting in poor formability. Increasing the temperature enables the formability of the alloy to be increased, with the exception of cases with very high Ca content, where the addition of Zn should be considered. This last point should be studied in further detail in future work.

4. Conclusion

This study focused on the deformation behavior of Mg-Ca(-Zn) alloys, which are promising candidates for biomedical applications. The microstructure of the alloys consisted of a solid solution of Mg and Mg_2Ca intermetallic phases as well as complex MgCaZn phases when Zn was added. The fraction of each phase and spatial distribution were dependent on the nominal composition. The high-temperature compression behavior of the Mg–Ca(–Zn) alloys was studied at different temperatures and strain rates. Classical viscoplastic behavior was observed. For higher Ca content, the alloy strength increased but the ductility decreased. DRX was described for the first time in a complex microstructure with two phases in a large amount. The evolution of the phases during the high-temperature evolution was monitored. From these results, a formability map was constructed that revealed that a higher Ca content resulted in a higher temperature and lower strain rate being required to be able to shape the alloy. Moreover, when Zn addition was considered, only a low strain rate and low temperature could be applied to enable deformation of the alloys. This finding is a key result for the future application of Mg-Ca(-Zn) alloys. It would be also interesting, as a perspective, to extend the formability map to check the possibility to shape these alloys at lower temperature. It will permit an easier industrial processing. This will constitute the topic of a future paper.

5. Data availability

The raw/processed data required to reproduce these findings cannot be shared at this time because of technical or time limitations.

6. References

[1] L. Liu, H. Zhou, Q. Wang, Y. Zhu, and W. Ding. Dynamic recrystallization behavior of AZ61 Magnesium alloy. *Advances in Technology of Materials and Materials Processing Journal*, 6(2):158–165, 2004.

[2] M. Hradilová, D. Vojtěch, J. Kubásek, J. Čapek, and M. Vlach. Structural and mechanical characteristics of Mg–4Zn and Mg–4Zn–0.4Ca alloys after different thermal and mechanical processing routes. *Materials Science & Engineering A*, 586:284–291, 2013.

[3] L.B. Tong, M.Y. Zheng, D.P. Zhang, W.M. Gan, H.G. Brokmeier, J. Meng, and H.J. Zhang. Compressive deformation behavior of Mg–Zn–Ca alloy at elevated temperature. *Materials Science & Engineering A*, 586:71–77, 2013.

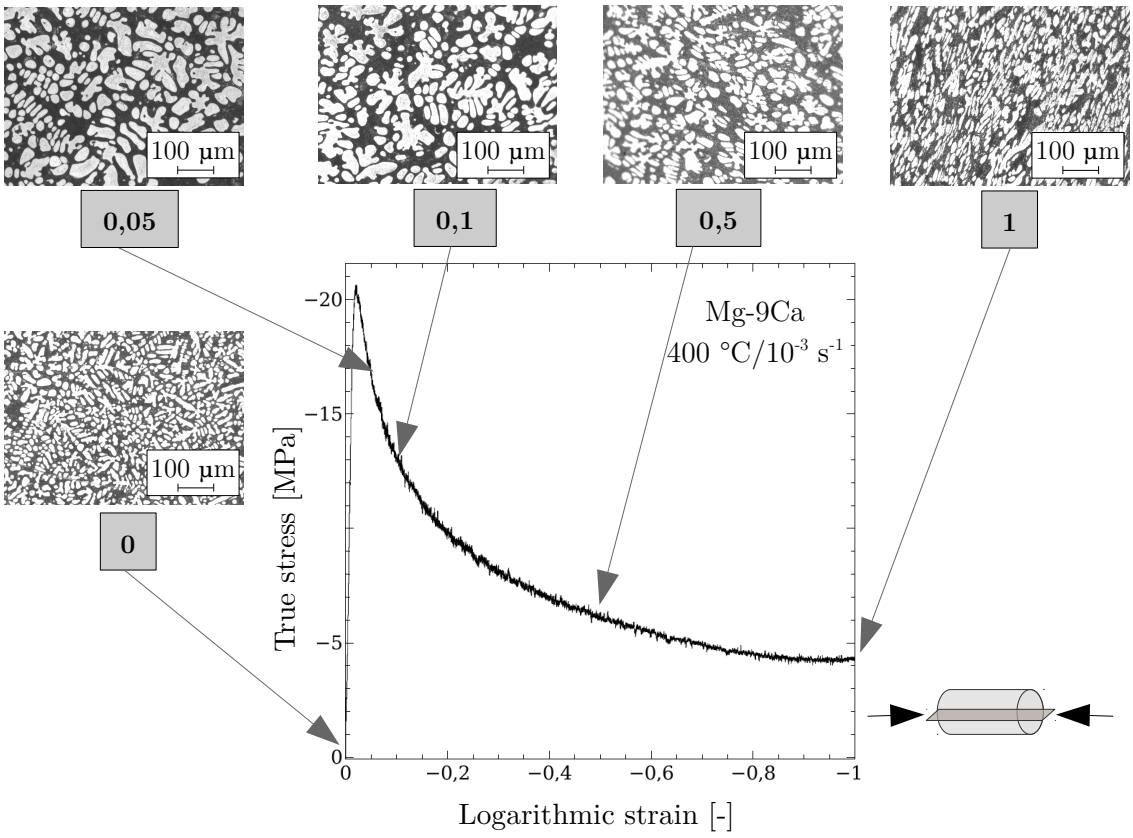

Figure 11: Evolution of the microstructure of Mg-9Ca alloy at 400 °C and 10^{-3} s^{-1}. Optical micrographs in the longitudinal direction of compression.

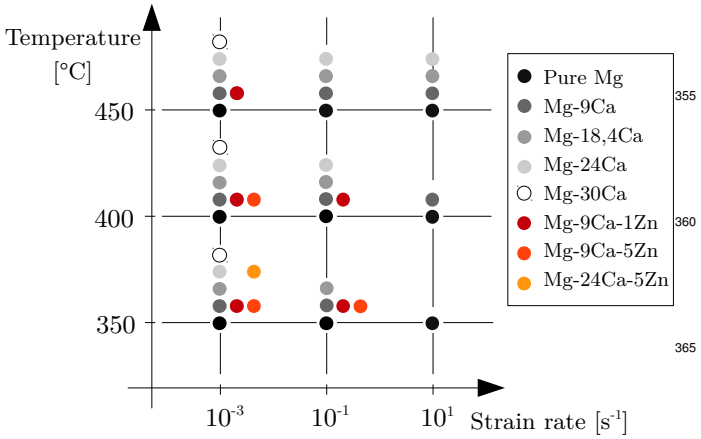

Figure 12: Formability of alloys as a function of temperature and strain rate.

[4] M. Hradilová, F. Montheillet, A. Fraczkiewicz, C. Desrayaud, and P. Lejček. Effect of Ca-addition on dynamic recrystallization of Mg–Zn alloy during hot deformation. *Materials Science & Engineering A*, 580:217–226, 2013.

[5] E. Zhang and L. Yang. Microstructure, mechanical properties and biocorrosion properties of Mg–Zn–Mn–Ca alloy for biomedical application. *Materials Science & Engineering A*, 497:111–118, 2008.

[6] S.M. Fatemi-Varzaneha, A. Zarei-Hanzakia, and H. Beladi. Dynamic recrystallization in AZ31 magnesium alloy. *Materials Science & Engineering A*, 456:52–57, 2007.

[7] T. Al-Samman and G. Gottstein. Dynamic recrystallization during high temperature deformation of magnesium. *Materials Science & Engineering A*, 490:411–420, 2008.

[8] J.C. Tan and M.J. Tan. Dynamic continuous recrystallization characteristics in two stage deformation of Mg - 3Al - 1Zn alloy sheet. *Materials Science & Engineering A*, 339:124–132, 2003.

[9] X. Fan, W. Tang, S. Zhang, D. Li, and Y. Peng. Effects of dynamic recrystallization in extruded and compressed AZ31 magnesium alloy. *Acta Metallurgica Sinica (English Letters)*, 23(5):334–342, 2010.

[10] H.T. Zhou, X.Q. Zeng, Q.D. Wang, and W.J. Ding. A flow stress model for AZ61 magnesium alloy. *Acta Metallurgica Sinica (English Letters)*, 17(2):155–160, 2004.

[11] H.T. Zhou, L.F. Liu, Q.D. Wang, D. Lu, X.Q. Zeng, and W.J. Ding. Strain softening and hardening behavior in AZ61 magnesium alloy. *Journal of Materials Science and Technology*, 20(6):691–693, 2004.

[12] M. Talebi Anaraki, M. Sanjari, and A. Akbarzadeh. Modeling of high temperature rheological behavior of AZ61 Mg-alloy using inverse method and ANN. *Materials and Design*, 29:1701–1706, 2008.

[13] X.-Y. Yang, Z.-S. Ji, H. Miura, and T. Sakai. Dynamic recrystallization and texture development during hot deformation of magnesium alloy AZ31. *Transactions of Nonferrous Metals Society of China*, 19:55–60, 2009.

[14] W.-J. Kim, S.W. Chung, C.S. Chung, and D. Kum. Superplasticity in thin magnesium alloy sheets and deformation mechanism maps for magnesium alloys at elevated temperatures. *Acta Materialia*, 49:3337–3345, 2001.

[15] T. Mohri, M. Mabuchi, M. Nakamura, T. Asahina, H. Iwasaki, T. Aizawa, and K. Higashi. Microstructural evolution and superplasticity of rolled Mg-9Al-1Zn. *Materials Science & Engineering A*, 290:139–144, 2000.

[16] Q. Wang, Y. Wei, Y. Chino, and M. Mabuchi. High strain rate superplasticity of rolled AZ91 magnesium alloy. *Rare Metals*, 27(1):46–49, 2008.

[17] A. Galiyev and R. Kaibyshev. Superplasticity in a magnesium alloy subjected to isothermal rolling. *Scripta Materialia*, 51:89–93, 2004.

[18] A. Galiyev, R. Kaibyshev, and G. Gottstein. Correlation of plastic de-

formation and dynamic recrystallization in magnesium alloy ZK60. *Acta Materialia*, 49:1199–1207, 2001.

[19] K.-D. Liss, T. Schmoelzer, K. Yan, M. Reid, M. Peel, R. Dippenaar, and H. Clemens. In situ study of dynamic recrystallization and hot deformation behavior of a multiphase titanium aluminide alloy. *Journal of Applied Physics*, 106(11), 2009.

[20] K.T. Conlon and D.S. Wilkinson. Effect of particle distribution on deformation and damage of two-phase alloys. *Materials Science & Engineering A*, 317:108–114, 2001.

[21] M. Salahshoor and Y. Guo. Biodegradable Orthopedic Magnesium-Calcium (MgCa) Alloys, Processing, and Corrosion Performance. *Materials*, 5(1):135–155, 2012.

[22] P. Salero. *Élaboration et caractérisation d'alliages Mg-Ca pour un procédé de minéralisation de l'eau par attaque électrochimique*. PhD thesis, Université de Lyon, 2015.

[23] E. Maire, P. Colombo, J. Adrien, L. Babout, and L. Biasetto. Characterization of the morphology of cellular ceramics by 3D image processing of X-ray tomography. *Journal of the European Ceramic Society*, 27(4):1973–1981, 2007.

[24] J. Schindelin, I. Arganda-Carreras, E. Frise, V. Kaynig, M. Longair, T. Pietzsch, S. Preibisch, C. Rueden, S. Saalfeld, B. Schmid, J.-Y. Tinevez, D.J. White, V. Hartenstein, K. Eliceiri, P. Tomancak, and A. Cardona. Fiji: an open-source platform for biological-image analysis. *Nature Methods*, 9(7):676–682, 2012.